ACS Sustainable Chemistry & Engineering

pubs.acs.org/journal/ascecg

Research Article

Intriguing Thermal Degradation Behavior of Aqueous Piperazine for Carbon Dioxide Capture: A First-Principles Assessment

Bohak Yoon and Gyeong S. Hwang*

Cite This: *ACS Sustainable Chem. Eng.* 2022, 10, 9584−9590

Read Online

ACCESS | Metrics & More | Article Recommendations | Supporting Information

ABSTRACT: Thermal degradation of aqueous piperazine (PZ) for CO_2 capture is experimentally known to yield a major product *N*-(2-aminoethyl)piperazine (AEP) and a minor product pair 1,1′-(1,2-ethanediyl)bis-piperazine (PEP) plus ethylenediamine (EDA), although the two reactions exhibit no substantial difference in thermodynamic favorability. This raises a question on factors affecting the rates of key reactions involved in PZ thermal degradation. Herein, we present the underlying mechanisms of PZ degradation and the relative rates of key steps involved based on ab initio metadynamics simulations. We have identified the reaction between PZ and protonated PZ resulting in an intermediate, 1-[2-(2-aminoethyl)amino]ethyl] piperazine ($AEAEPZH^+$), and the subsequent reaction of $AEAEPZH^+$ with PZ leading to AEP or PEP/EDA. Our simulations demonstrate that the free-energy barriers for these intermolecular reactions are largely determined by the local solvation structure and dynamics of the amine species involved. We also discuss the strong effects of temperature and molecular structure on the solvation environments. While offering an explanation for preferred AEP formation in 30 wt % PZ, our work sheds light on the possibility that both the mechanism and rate of the PZ degradation reaction can be altered with changes in temperature and amine concentration.

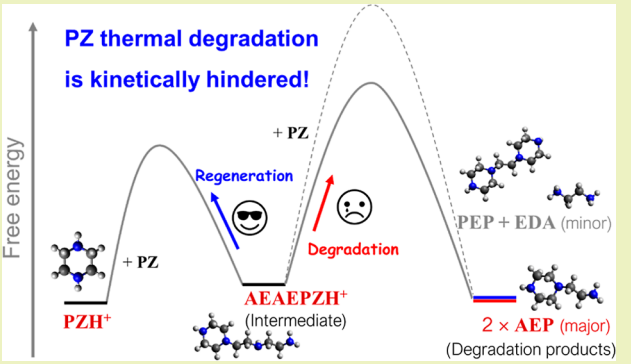

KEYWORDS: *piperazine, thermal degradation, CO_2 capture, ab initio molecular dynamics, metadynamics*

INTRODUCTION

Increasing greenhouse gas emissions are commonly believed to have caused global climate changes over the last century.[1,2] Carbon dioxide (CO_2) is one of the major greenhouse gases; hence, there have been significant efforts to mitigate its emissions.[3,4] Amine-based scrubbing is currently a commercially promising option for post-combustion CO_2 capture from flue gases.[4,5] However, its wide practical application tends to be hindered by some drawbacks including high energy consumption, degradation, and corrosion.[6−8] Particularly, parasitic reactions that lead to amine degradation raise serious issues regarding solvent loss, detrimental compound formation, and/or material corrosion.[6,9,10] Amine reclamation may contribute about 10% to the total cost of CO_2 capture.[11,12] Moreover, some degradation products are known to be possibly dangerous if released into the environment.[13] Hence, it is imperative to have an in-depth understanding of the mechanisms and dynamics of amine degradation reactions.

Piperazine (PZ), a cyclic compound containing two secondary amine groups, is known to be advantageous over conventional alkanolamines such as monoethanolamine (MEA) due to its higher resistance to degradation and corrosion, besides its higher capacity for CO_2 absorption and lower energy for regeneration.[14,15] Nonetheless, PZ has been experimentally reported to undergo thermal degradation mainly during CO_2 stripping at high temperatures of 140−150 °C.[16,17]

From previous experiments, the major products from thermal degradation of CO_2-loaded aqueous PZ have been identified to be *N*-(2-aminoethyl)piperazine (AEP), 1,1′-(1,2-ethanediyl)bis-piperazine (PEP), and ethylenediamine (EDA), in the order from largest to smallest concentrations.[15,18] 1-[2-[(2-Aminoethyl)amino]ethyl] piperazine (AEAEPZ) and protonated AEAEPZ ($AEAEPZH^+$) have been proposed to be key intermediates, due to their small quantities identified, that lead to the major degradation products.[19] Very recently, Parks and co-workers have reported the predicted formation enthalpies of several products from PZ thermal degradation based on quantum mechanical (QM) calculations with an implicit solvent model.[20] However, some fundamental aspects of the PZ degradation reactions still remain unclear.

Received: April 27, 2022
Revised: July 1, 2022
Published: July 14, 2022

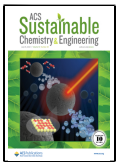

In this study, we examine the mechanisms underlying the PZ thermal degradation reactions in a CO_2-loaded aqueous solution. We first use implicit solvent model calculations to assess possible degradation pathways based on the predicted relative stabilities of products and intermediates. Thereafter, we employ ab initio molecular dynamics (AIMD) coupled with metadynamics sampling to calculate the free-energy barriers for key elementary reactions. We also discuss the underlying factors responsible for the predominant production of AEP over PEP + EDA as well as the strong temperature dependence of the degradation rates and pathways, through analyses of the solvation structure and dynamics along with hydrogen bond dynamics.

COMPUTATIONAL METHODS

Static QM calculations were carried out with the Gaussian 16 program at the theory level of B3LYP/6-311++G(d,p).[21] Here, the free energies of solvation for all species considered were calculated with the solvation model based on density (SMD) developed by Truhlar and co-workers;[22] the vibrational contribution to the free energy was assessed by calculating harmonic frequencies. The computational methodologies used have been verified and confirmed to be appropriate for the study of reactions in CO_2-loaded amine solutions.[23−26] Density functional theory-based AIMD simulations were carried out using the Car−Parrinello Molecular Dynamics (CPMD) software.[27] A fictitious electron mass of 550 a.u. was used. We employed revised Perdew, Berke, and Ernzerhof functionals[28,29] and also verified that the conclusions drawn upon the results on this work are not affected by the choice of functionals (see the Supporting Information). Norm-conserving pseudopotentials by Troullier−Martins[30] with the treatment of the non-local part by Kleinman−Bylander transformation[31] were implemented to depict the interactions between the core and valence electrons. A plane-wave basis set with an energy cutoff of E_{cut} = 700 eV was used. Using Grimme's semiempirical corrections,[32] long-range van der Waals interactions were included in determining the structure of liquid water.[33] All AIMD simulations were conducted in the canonical (*NVT*) ensemble with a timestep of 0.12 fs. Under the velocity Verlet algorithm, the integration parameter developed by Yoshida-Suzuki[34] with a value of 4.0 was employed. A Nose−Hoover thermostat with a damping parameter of 200 fs was implemented for temperature control.[35] Given the lack of structural symmetry in the aqueous system, only the gamma (Γ) point was considered to sample the Brillouin zone. The convergence with respect to E_{cut} and *k*-points was cautiously tested (see the Supporting Information). The deuterium mass was used for hydrogen atoms, allowing a relatively larger electronic mass and a longer timestep by effectively decoupling the electronic and ionic degrees of freedom. With the PLUMED package[36] implemented in the CPMD code, well-tempered metadynamics simulations[37,38] were implemented to calculate free-energy profiles for the reactions examined. During metadynamics simulations, Gaussian hills with an initial hill height of 1.15 kcal/mol and a width of 0.03 Å were added at a rate of 10^{-4} fs^{-1} with the height decrease controlled by a bias factor of 15 yielding ΔT = 4700 K (when T = 313 K) and ΔT = 6200 K (when T = 413 K). Prior to production runs, every system was fully equilibrated for at least 10 ps under the *NVT* ensemble. More details on the verification of transition states (TSs) and convergence of metadynamics simulations are discussed in the Supporting Information (see the Supporting Information).

RESULTS AND DISCUSSION

Thermodynamic Assessment of PZ Degradation Pathways. As shown in Figure 1, we first assessed the relative thermodynamic stabilities of major species possibly generated during PZ thermal degradation with respect to PZ and CO_2, based on QM implicit-solvent calculations. According to previous studies,[39] PZ may react with CO_2 forming a carbamate ($PZCOO^-$), accompanied by a release of a proton (H^+). The released H^+ may be abstracted by a free PZ forming a protonated PZ (PZH^+) or a COO^- moiety in a carbamate forming a carbamic acid (PZCOOH). Our calculations predict the former, that is, 2 PZ + CO_2 → $PZCOO^-$ + PZH^+ (ΔG_{aq} = −0.7 kcal/mol), to be slightly more thermodynamically favorable than the latter, that is, 2PZ + CO_2 → PZCOOH + PZ (ΔG_{aq} = 2.2 kcal/mol). This can be understandable considering that PZ is more basic than $PZCOO^-$, thus $PZCOO^-$/PZH^+ pair formation has been found to prevail over PZCOOH formation.[14]

Once formed, PZH^+ may react with free PZ leading to reactive $AEAEPZH^+$ intermediate formation, that is, PZH^+ +

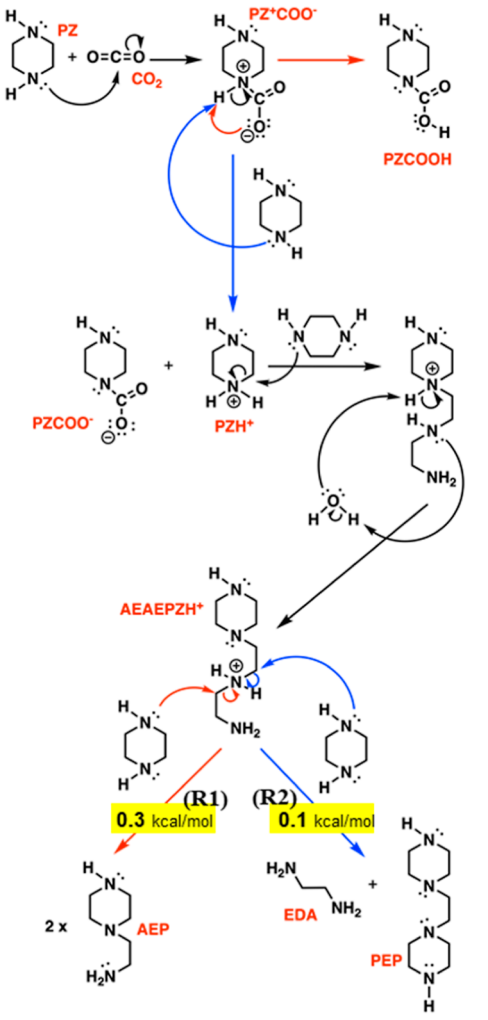

	ΔH^0_{aq}	ΔG^0_{aq}
2 PZ + CO_2 → $PZCOO^-$ + PZH^+	-9.4	-0.7
2 PZ + CO_2 → PZCOOH + PZ	-6.7	2.2
PZ + PZH^+ → $AEAEPZH^+$	-2.1	2.5
PZ + $AEAEPZH^+$ → 2 AEP	-0.3	0.3
PZ + $AEAEPZH^+$ → PEP + EDA	-0.7	0.1

Figure 1. Predicted Gibbs free-energy changes (ΔG_{aq} in kcal/mol) for the key elementary reactions considered in thermal degradation of aqueous piperazine (PZ). Reactants, isolated CO_2 and PZ in aqueous solution, are indicated as a reference (ΔG_{aq} = 0).

https://doi.org/10.1021/acssuschemeng.2c02502
ACS Sustainable Chem. Eng. 2022, 10, 9584−9590

PZ → AEAEPZH$^+$, which is predicted to be an endergonic reaction (ΔG_{aq} = 2.5 kcal/mol). Subsequently, AEAEPZH$^+$ may undergo a reaction with PZ as described in the following paragraph or release a proton to form AEAEPZ. We also considered the possibility of urea formation from the reaction between PZ and PZCOOH (PZ + PZCOOH → urea + H_2O), as reported in the cases of MEA and EDA.[23,40] Our calculation predicts the urea formation reaction to be endergonic (ΔG_{aq} = 4.2 kcal/mol) while requiring overcoming a very high free-energy barrier of $\Delta A^{\ddagger}$ = 42.2 kcal/mol. This implies the unlikelihood of it occurring, which is consistent with previous experimental observations;[17] hence, urea formation was ruled out in the further analysis.

The reaction of AEAEPZH$^+$ with PZ may follow one of two routes that involve nucleophilic substitution, in which a nucleophilic nitrogen (N) atom of PZ attacks either of the two electrophilic carbon (C) atoms bonded to the protonated N in AEAEPZH$^+$,[19] as illustrated in Figures 1 and 5:

(R1) Formation of AEP and AEPH$^+$ (AEAEPZH$^+$ + PZ → AEP + AEPH$^+$) is predicted to be an endergonic reaction (ΔG_{aq} = 0.8 kcal/mol); AEPH$^+$ may subsequently release a proton (ΔG_{aq} = −0.5 kcal/mol), thus this reaction would yield two stable AEP molecules per AEAEPZH$^+$.

(R2) Formation of PEPH$^+$ and EDA (AEAEPZH$^+$ + PZ → PEPH$^+$ + EDA) is also predicted to be an endergonic reaction (ΔG_{aq} = 1.1 kcal/mol); PEPH$^+$ may subsequently release a proton (ΔG_{aq} = −1.0 kcal/mol), thus this reaction would yield stable PEP and EDA molecules per AEAEPZH$^+$.

Given the comparable ΔG_{aq}, the two routes could be considered nearly equally favorable from the perspective of thermodynamics. However, according to experimental observations, AEP is the predominant product of thermal degradation of aqueous PZ loaded with CO_2. This implies that kinetics may greatly contribute to determining the thermal degradation mechanisms, as demonstrated in our prior work.[23−25,40] Molecular mechanisms underlying the reactions of aqueous amine solvents for CO_2 capture have been found to be often governed by the relative rates of competing reactions (kinetics), instead of the comparative stabilities of products and intermediates (thermodynamics). We evaluate the relative rates of a few key reactions involved in PZ thermal degradation by computing their free-energy barriers in the following sections.

AEAEPZH$^+$ Intermediate Formation. Metadynamics simulations were performed at two different temperatures, 313 and 413 K, to examine the temperature dependence of the free-energy barrier for AEAEPZH$^+$ formation from the reaction of PZ with PZH$^+$. 30H_2O, 1PZH$^+$, 1PZ, and 1PZCOO$^-$ molecules were put in the periodic simulation box with a cubic edge length of 12.1 Å, which corresponds to about 27 wt % PZ solution at 0.33 CO_2 loading. As illustrated in Figure 2, this reaction involves the ring opening of PZH$^+$ by PZ; that is, the bond between the protonated N (denoted by N*) and adjacent electrophilic C (C*) atoms in PZH+ is cleaved due to nucleophilic attack by a lone pair on N of nearby PZ on the C* atom. The nucleophilic substitution reaction was described by a single collective variable (CV) of a linear combination of two independent bond distances, $d_{N-C^*}-d_{N^*-C^*}$, (where d_{N-C^*} is the distance between the N of PZ and the C* of PZH$^+$ and $d_{N^*-C^*}$ is the distance of the N*−C* bond being broken in PZH$^+$).

Figure 2 shows the predicted free-energy barriers for the PZH$^+$ + PZ → AEAEPZH$^+$ reaction at 313 and 413 K, along

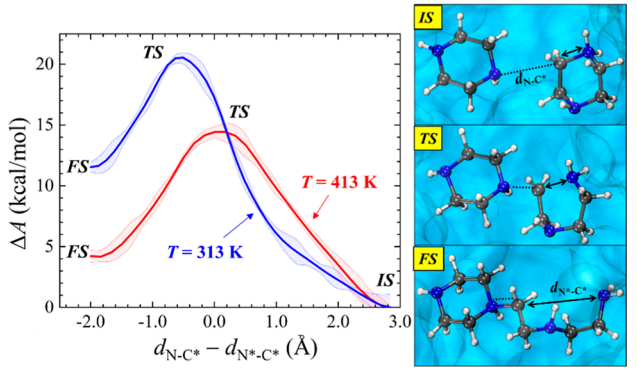

Figure 2. Free-energy barriers (ΔA in kcal/mol) for the formation of AEAEPZH$^+$ from the reaction between PZ and PZH$^+$, that is, PZ + PZH$^+$ → AEAEPZH$^+$, predicted by CPMD-metadynamics simulations at 313 and 413 K as specified. Shown at right are the molecular configurations of IS, TS, and FS, in which N, O, C, and H atoms are denoted by blue, red, gray, and white balls, respectively.

with the structural changes associated. In the initial state (IS), PZ and PZH$^+$ are separated with d_{N-C^*} = 4.15 Å and $d_{N^*-C^*}$ = 1.25 Å, yielding a CV value of 2.9 Å, at both 313 and 413 K. As the lone pair of N in PZ interacts with the C* atom in PZH$^+$, the N*−C* bond is elongated. As such, d_{N-C^*} and $d_{N^*-C^*}$ become 1.42 (1.61) Å and 1.92 (1.51) Å in the TS at 313 K (413 K), respectively, yielding a CV value of −0.5 (0.1) Å. It is also worth noting the noticeable difference between the TS configurations at 313 and 413 K, indicative of the strong temperature-dependence of an intermolecular reaction in aqueous amine solutions.[24,25] The final state (FS) at both 313 and 413 K gives 1.52 Å of d_{N-C^*} and 3.43 Å of $d_{N^*-C^*}$; the resulting large negative CV value of −1.9 Å represents the open ring structure of AEAEPZH$^+$.

The free-energy barrier for the PZ + PZH$^+$ → AEAEPZH$^+$ reaction is predicted to be 20.9 kcal/mol at 313 K and decreases to 14.1 kcal/mol at 413 K; the respective return barriers are 10.1 and 10.4 kcal/mol. The lower barrier at 413 K may suggest that the thermal degradation of PZ via AEAEPZH$^+$ formation could be substantially facilitated at high stripping temperatures as compared to that at low absorbing temperatures, consistent with existing experimental observations.[19] The underlying mechanism responsible for the strong temperature dependence of AEAEPZH$^+$ formation will be discussed in the following section.

Like the cases shown in our previous studies,[24,25,40] the intermolecular interaction leading to AEAEPZH$^+$ formation can be largely determined by the solvation structure and dynamics of PZ and PZH$^+$. For a better understanding of the temperature effect, we analyzed their solvation behaviors at different temperatures. First, we computed the MSDs of water molecules surrounding PZ and PZH$^+$. Here, MSD is given by $|R_i(t) - R_i(0)|^2$, where $R_i(t)$ and $R_i(0)$ are the positions of atom i at time t and 0, respectively. As shown in Figure 3a, the water molecules are evidently more mobile at 413 K than at 313 K, enhancing the interaction between PZ and PZH$^+$.

To gain a deeper insight into the dynamic nature of the surrounding water molecules, we also evaluated their reorientational dynamics by computing the time correlation function. The water reorientation correlation function is defined as

$$C_{\boldsymbol{u}}^{(2)}(t) = \frac{\langle P_2[\boldsymbol{u}(t)\cdot\boldsymbol{u}(0)]\rangle}{\langle P_2[\boldsymbol{u}(0)\cdot\boldsymbol{u}(0)]\rangle} \quad (1)$$

https://doi.org/10.1021/acssuschemeng.2c02502
ACS Sustainable Chem. Eng. 2022, 10, 9584−9590

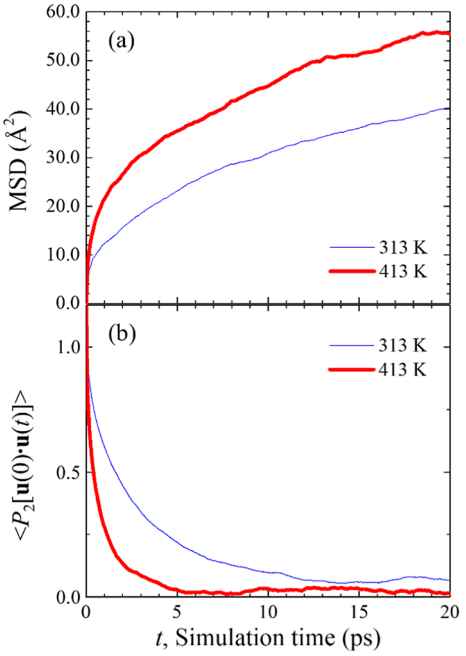

Figure 3. (a) Mean-square displacement (MSD) and (b) reorientation time-correlation function of water molecules between PZ and PZH^+ at 313 K (thin blue line) and 413 K (thick red line).

where the angle bracket represents an ensemble and time average of the unit vector, P_2 is the second-rank Legendre polynomial, and $\boldsymbol{u}(t)$ and $\boldsymbol{u}(0)$ are the unit vectors along the dipole moment of the water molecules (representing the molecular orientation at times t and 0, respectively). The water dipole moment is computed with maximally localized Wannier functions (MLWFs). Considering the MLWF centers are treated as quasiparticles, the locations and charges of the nuclei and the centers of MLWFs are integrated to determine the dipole moment. As illustrated in Figure 3b, the water reorientation is found to occur much faster at 413 K than at 313 K, consistent with its higher mobility as predicted earlier.

We also calculated the pair distribution function (PDF) between N in PZ and C* in PZH^+ (which are directly involved in the formation of $AEAEPZH^+$) using AIMD simulations. The PDF is defined by $g(r) = \langle n(r, r + dr)/4\pi r^2 \rho dr \rangle$, where ρ is the bulk number density, and $n(r, r + dr)$ denotes the number of C* atom in a spherical shell of radius r with a thickness r from the reference N atom (or, vice versa). The $g(r)$ was obtained from the average of five independent runs with different starting configurations. As shown in Figure 4, two distinct peaks appear around 6.0 and 7.6 Å at 413 K, implying that one or two water molecules may exist between the N and C* atoms. On the other hand, the first peak appears around 7.7 Å at 313 K, suggesting the presence of at least two water molecules hindering the interaction between N in PZ and C* in PZH^+.

Our analyses clearly demonstrate the strong temperature dependence of solvation dynamics in the aqueous PZ/PZH^+ system. The solvating water molecules become more mobile and less rigidly organized with increasing temperature, thereby enhancing the interaction between N in PZ and C* in PZH^+. This could explain why the free-energy barrier for the PZ + PZH^+ → $AEAEPZH^+$ reaction substantially drops as the temperature increases from 313 to 413 K.

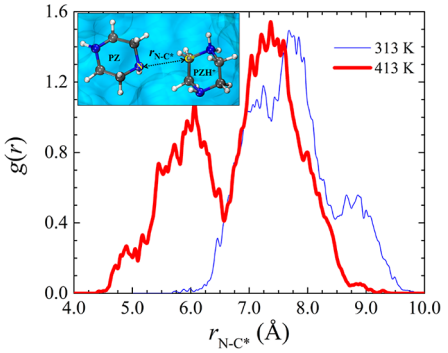

Figure 4. PDFs, $g(r)$, between N in PZ and C* of PZH^+, from AIMD simulations at 313 K (thin blue line) and 413 K (thick red line). Shown in the inset are the associated molecular configurations, in which the blue, gray, and white balls represent N, C, and H atoms, respectively.

Kinetic Competitions for AEP versus PEP + EDA Formations from $AEAEPZH^+$. As described earlier, the predominant formation of AEP over PEP + EDA from the reaction of $AEAEPZH^+$ with PZ could not be explained in terms of thermodynamic favorability. Hence, we evaluated the relative rates of the two competing reactions by calculating their free-energy barriers using metadynamics simulations at two different temperatures (313 and 413 K). Here, the two electrophilic C atoms bonded to the protonated N (referred to as N*) in $AEAEPZH^+$ are denoted by C_6 and C_7, respectively; recall that AEP (PEP + EDA) formation involves the nucleophilic attack of N of PZ on the C_7 (C_6) atom, as shown in Figure 5. The nucleophilic substitution reaction was described with a single CV, $d_{N-Ci}-d_{N^*-Ci}$; here, d_{N-Ci} represents the distance between the N in PZ and the C_i (i = 6 or 7) in $AEAEPZH^+$, and d_{N^*-Ci} is the distance of the N^*-C_i bond in $AEAEPZH^+$. CPMD-metadynamics simulations were carried out under periodic boundary conditions with a cubic simulation box of 12.15 Å side length, containing 1 PZ, 1 $AEAEPZH^+$, and 40 water molecules.

As shown in Figure 5, the IS indicates d_{N-Ci} = 3.24 Å, and d_{N^*-Ci} = 1.54 Å, yielding a CV of 1.7 Å (= $d_{N-Ci}-d_{N^*-Ci}$); the relatively large positive value of CV indicates that PZ and $AEAEPZH^+$ are separated with no significant interaction. In the TS, d_{N-Ci} decreases to 2.41 Å, while d_{N^*-Ci} increases to 2.63 Å, implying that the nucleophilic attack of PZ weakens and elongates the N^*-C_i bonds in AEAEPZH. In the *FS*, d_{N-Ci} further decreases to 1.51 Å, and d_{N^*-Ci} becomes 3.60 Å, indicating $N-C_i$ bond formation and N^*-C_i bond scission. The predicted free-energy barrier for the nucleophilic substitution reaction leading to AEP formation is 17.1 (7.9) kcal/mol at 313 (413) K, and that leading to PEP + EDA formation is 34.9 (23.2) kcal/mol. The substantial free-energy barrier difference clearly demonstrates that the AEP formation can be much more kinetically favorable than the PEP + EDA formation. This result evidently supports the experimental observations that the major thermal degradation product by far is AEP with EDA/PEP minor products in CO_2-loaded aqueous PZ.

It is also worth noting that the free-energy barriers for both cases significantly reduce with increasing temperature; the temperature dependence tends to be even stronger when compared with the case of $AEAEPZH^+$ formation. Therefore, the rate-determining step for the PZ thermal degradation is likely to be temperature dependent; that is, the predicted free-

https://doi.org/10.1021/acssuschemeng.2c02502
ACS Sustainable Chem. Eng. 2022, 10, 9584−9590

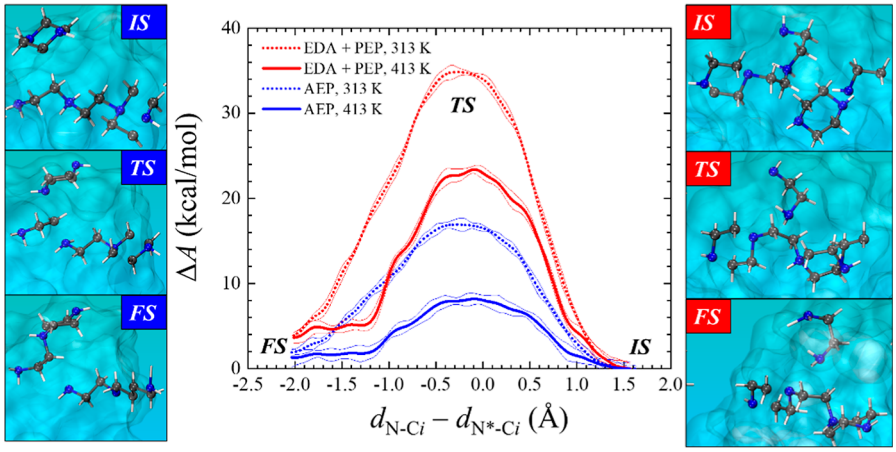

Figure 5. Free-energy barriers (ΔA in kcal/mol) for the formation of AEP (in blue) and of EDA + PEP (in red) from the reaction between PZ and AEAEPZH$^+$, that is, PZ + AEAEPZH$^+$ → 2 AEP, and that is, PZ + AEAEPZH$^+$ → EDA + PEP, predicted by CPMD-metadynamics simulations at 313 K (in dotted line) and 413 K (in solid line). Shown at the left and right are the molecular configurations of IS, TS, and FS, in which N, O, C, and H atoms are denoted by blue, red, gray, and white balls, respectively.

energy barrier for AEAEPZH$^+$ intermediate formation is noticeably higher than that for its subsequent reaction at 413 K, while the opposite is true at 313 K. This reiterates the importance of understanding temperature-dependent kinetics and the reaction mechanism for the PZ thermal degradation, while predicting the PZH$^+$ + PZ → AEAEPZH$^+$ reaction to be a rate-controlling step at high stripping temperatures.

To evaluate the solvation effect on the intermolecular PZ + AEAEPZH$^+$ reaction, we assessed the interaction of water with the electrophilic C_6 and C_7 atoms in AEAEPZH$^+$. The life-time autocorrelation function, $C_{X-W}(t)$, for the binary interaction between C_6 or C_7 (in AEAEPZH$^+$) and O_W (in nearby water) may indicate how long individual water molecules stay near the C_6 or C_7 site. From the predicted correlation functions in Figure 6, the average life-time (τ_C) of the C_6–O_W (C_7–O_W)

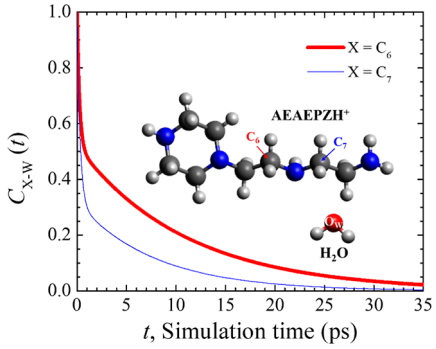

Figure 6. Life-time autocorrelation functions for the C_6–O_w (thick red line) and C_7–O_w (thin blue line) pairs for AEAEPZH$^+$ from AIMD simulations at 313 K. N, O, C, and H atoms are denoted by blue, red, gray, and white balls, respectively.

interaction is estimated to be 10.1 (5.7) ps. The longer τ_C implies that water molecules may more strongly interact with the C_6 atom; thus, the interaction between C_6 and N (in PZ) could be more hindered than the C_7–N interaction. We also compared the pairwise interactions between N in PZ and C_i (i = 6, 7) in AEAEPZH$^+$. As shown in Figure 7, the N–C_6 and N–C_7 PDFs exhibit a distinct first peak around 5.0 and 7.0 Å, respectively, which may imply the presence of at least one water molecule (two water molecules) between the N and C_6

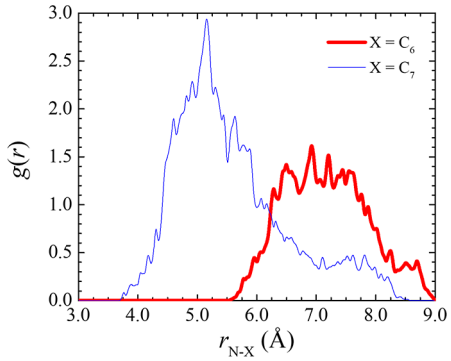

Figure 7. PDFs, $g(r)$, between N in PZ and C_6 (thick red line) or C_7 (thin blue line) of AEAEPZH$^+$ at 313 K from AIMD simulations.

(C_7) atoms. These analyses evidently demonstrate that the C_7 site is more accessible to the N of PZ, which can be primarily responsible for the reduced free-energy barrier. As such, the kinetic preference for the nucleophilic substitution reaction leading to AEP formation provides an explanation for the predominant production of AEP over PEP/EDA during thermal degradation of CO_2-loaded aqueous PZ.

CONCLUSIONS

We investigated the thermal degradation of aqueous PZ solution for CO_2 capture, from both thermodynamics and kinetics perspectives, using first-principles computational methods. Our key results are recapitulated as follows:

- The PZ thermal degradation is initiated by the reaction of PZH$^+$ with PZ leading to reactive AEAEPZH$^+$ intermediate formation. The predicted free-energy barrier for this reaction substantially drops from 20.9 to 14.1 kcal/mol as the temperature increases from 313 to 413 K. Our analysis shows that the strong temperature dependence is primarily attributed to the fact that the water molecules solvating the reactants become more mobile and less rigidly organized with increasing temperature, thereby enhancing the intermolecular reaction.
- The reaction of AEAEPZH$^+$ with PZ may lead to the formation of an AEP or PEP + EDA pair. While the two

https://doi.org/10.1021/acssuschemeng.2c02502
ACS Sustainable Chem. Eng. 2022, 10, 9584–9590

competing reactions appear to be nearly equally favorable from a thermodynamic point of view, the former has a substantially lower free-energy barrier (~7.9 kcal/mol) than the latter (~23.3 kcal/mol) at 413 K due to the solvation effects; the free-energy barriers for both reactions increase with decreasing temperature. This suggests that the PZ degradation process is largely controlled by kinetics rather than thermodynamics, while providing a convincing explanation for the experimental observation of predominant production of AEP over PEP/EDA.

- While the free-energy barriers for the intermolecular reactions examined are sensitive to temperature, the rate-determining step for the PZ thermal degradation is likely to be temperature-dependent. At high stripping temperatures (~413 K), the $PZH^+ + PZ \rightarrow AEAEPZH^+$ reaction is predicted to be a rate-controlling step, whereas the subsequent reaction of $AEAEPZH^+$ with PZ is found to have a higher free-energy barrier at 313 K.

Our work sheds light on the importance of local solvation structure and dynamics of amine reactants and intermediates, which are mainly responsible for the temperature-dependent kinetics and the reaction mechanism for the PZ thermal degradation. The detailed understanding at the atomic level can greatly help to develop cost- and energy-efficient amine-based solvents for carbon capture.

■ ASSOCIATED CONTENT

Supporting Information

The Supporting Information is available free of charge at https://pubs.acs.org/doi/10.1021/acssuschemeng.2c02502.

Additional information on computational methodologies and supplementary calculations supporting the conclusions drawn upon in this work; sensitivity of choice of functionals; convergence of cutoff energy; sensitivity of *k*-point set; verification of identified TSs; and convergence of metadynamics simulations (PDF)

■ AUTHOR INFORMATION

Corresponding Author

Gyeong S. Hwang − *McKetta Department of Chemical Engineering, University of Texas at Austin, Austin, Texas 78712, United States;* orcid.org/0000-0002-5538-9426; Phone: 1-512-471-4847; Email: gshwang@che.utexas.edu; Fax: 1-512-471-7060

Author

Bohak Yoon − *McKetta Department of Chemical Engineering, University of Texas at Austin, Austin, Texas 78712, United States*

Complete contact information is available at: https://pubs.acs.org/10.1021/acssuschemeng.2c02502

Notes

The authors declare no competing financial interest.

■ ACKNOWLEDGMENTS

This work was supported by ExxonMobil, the Korea CCS R&D Center (KCRC) grant (no. 2017M1A8A1072016) funded by the Korea government (Ministry of Science, ICT & Future Planning), and the R.A. Welch Foundation (no. F-1535). We would like to thank Dr. David Calabro, Dr. Lisa Baugh, and Dr. Sumathy Raman at ExxonMobil for the helpful discussions and suggestions. We also acknowledge the Texas Advanced Computing Center (TACC) at the University of Texas at Austin for providing HPC resources that have contributed to the simulation results reported herein.

■ REFERENCES

(1) Bui, M.; Adjiman, C. S.; Bardow, A.; Anthony, E. J.; Boston, A.; Brown, S.; Fennell, P. S.; Fuss, S.; Galindo, A.; Hackett, L. A.; et al. Carbon Capture and Storage (CCS): The Way Forward. *Energy Environ. Sci.* **2018**, *11*, 1062−1176.

(2) Orr, J. C.; Fabry, V. J.; Aumont, O.; Bopp, L.; Doney, S. C.; Feely, R. A.; Gnanadesikan, A.; Gruber, N.; Ishida, A.; Joos, F.; et al. Anthropogenic Ocean Acidification over the Twenty-First Century and Its Impact on Calcifying Organisms. *Nature* **2005**, *437*, 681−686.

(3) Vasudevan, S.; Farooq, S.; Karimi, I. A.; Saeys, M.; Quah, M. C. G.; Agrawal, R. Energy penalty estimates for CO2 capture: Comparison between fuel types and capture-combustion modes. *Energy* **2016**, *103*, 709−714.

(4) Rochelle, G. T. Amine Scrubbing for CO 2 Capture. *Science* **2009**, *325*, 1652−1654.

(5) Figueroa, J. D.; Fout, T.; Plasynski, S.; McIlvried, H.; Srivastava, R. D. Advances in CO2 capture technology-The U.S. Department of Energy's Carbon Sequestration Program. *Int. J. Greenh. Gas Control* **2008**, *2*, 9−20.

(6) Strazisar, B. R.; Anderson, R. R.; White, C. M. Degradation Pathways for Monoethanolamine in a CO2 Capture Facility. *Energy Fuel.* **2003**, *17*, 1034−1039.

(7) Stowe, H. M.; Hwang, G. S. Fundamental Understanding of CO2 Capture and Regeneration in Aqueous Amines from First-Principles Studies: Recent Progress and Remaining Challenges. *Ind. Eng. Chem. Res.* **2017**, *56*, 6887−6899.

(8) D'Alessandro, D. M.; Smit, B.; Long, J. R. Carbon Dioxide Capture: Prospects for New Materials. *Angew. Chem., Int. Ed.* **2010**, *49*, 6058−6082.

(9) Abu-Zahra, M. R. M.; Schneiders, L. H. J.; Niederer, J. P. M.; Feron, P. H. M.; Versteeg, G. F. CO2 capture from power plants. *Int. J. Greenh. Gas Control* **2007**, *1*, 37−46.

(10) Damiani, D.; Litynski, J. T.; McIlvried, H. G.; Vikara, D. M.; Srivastava, R. D. The US department of Energy's R&D program to reduce greenhouse gas emissions through beneficial uses of carbon dioxide. *Greenhouse Gases: Sci. Technol.* **2012**, *2*, 9−16.

(11) Reynolds, A. J.; Verheyen, T. V.; Adeloju, S. B.; Meuleman, E.; Feron, P. Towards Commercial Scale Postcombustion Capture of CO2 with Monoethanolamine Solvent: Key Considerations for Solvent Management and Environmental Impacts. *Environ. Sci. Technol.* **2012**, *46*, 3643−3654.

(12) Rao, A. B.; Rubin, E. S. A Technical, Economic, and Environmental Assessment of Amine-Based CO2 Capture Technology for Power Plant Greenhouse Gas Control. *Environ. Sci. Technol.* **2002**, *36*, 4467−4475.

(13) Rochelle, G. T. Thermal degradation of amines for CO2 capture. *Curr. Opin. Chem. Eng.* **2012**, *1*, 183−190.

(14) Rochelle, G.; Chen, E.; Freeman, S.; Van Wagener, D.; Xu, Q.; Voice, A. Aqueous piperazine as the new standard for CO2 capture technology. *Chem. Eng. J.* **2011**, *171*, 725−733.

(15) Freeman, S. A.; Dugas, R.; Van Wagener, D. H.; Nguyen, T.; Rochelle, G. T. Carbon Dioxide Capture with Concentrated, Aqueous Piperazine. *Int. J. Greenh. Gas Control* **2010**, *4*, 119−124.

(16) Freeman, S. A.; Davis, J.; Rochelle, G. T. Degradation of Aqueous Piperazine in Carbon Dioxide Capture. *Int. J. Greenh. Gas Control* **2010**, *4*, 756−761.

(17) Freeman, S. A.; Rochelle, G. T. Thermal Degradation of Aqueous Piperazine for CO2 Capture. 1. Effect of Process Conditions and Comparison of Thermal Stability of CO2 Capture Amines. *Ind. Eng. Chem. Res.* **2012**, *51*, 7719−7725.

(18) Mazari, S. A.; Ali, B. S.; Jan, B. M.; Saeed, I. M. Degradation study of piperazine, its blends and structural analogs for CO2 capture: A review. *Int. J. Greenh. Gas Control* **2014**, *31*, 214−228.
(19) Freeman, S. A.; Rochelle, G. T. Thermal Degradation of Aqueous Piperazine for CO2 Capture: 2. Product Types and Generation Rates. *Ind. Eng. Chem. Res.* **2012**, *51*, 7726−7735.
(20) Parks, C.; Hughes, K.; Pourkashanian, M. Rationalizing Product Formation in Piperazine Degradation: A Computational Study. *Ind. Eng. Chem. Res.* **2021**, *60*, 12864−12882.
(21) Frisch, M. J.; Trucks, G. W.; Schlegel, H. B.; Scuseria, G. E.; Robb, M. A.; Cheeseman, J. R.; Scalmani, G.; Barone, V.; Mennucci, B.; Petersson, G. A.; et al. *Gaussian 16*; Gaussian, Inc.: Wallingord CT, 2010.
(22) Marenich, A. V.; Cramer, C. J.; Truhlar, D. G. Universal Solvation Model Based on Solute Electron Density and on a Continuum Model of the Solvent Defined by the Bulk Dielectric Constant and Atomic Surface Tensions. *J. Phys. Chem. B* **2009**, *113*, 6378−6396.
(23) Yoon, B.; Stowe, H. M.; Hwang, G. S. Molecular mechanisms for thermal degradation of CO2-loaded aqueous monoethanolamine solution: a first-principles study. *Phys. Chem. Chem. Phys.* **2019**, *21*, 22132−22139.
(24) Yoon, B.; Hwang, G. S. Anomalous Facile Carbamate Formation at High Stripping Temperatures from Carbon Dioxide Reaction with 2-Amino-2-Methyl-1-Propanol in Aqueous Solution. *ACS Sustain. Chem. Eng.* **2020**, *8*, 18671−18677.
(25) Yoon, B.; Hwang, G. S. First-Principles Assessment of Anomalous Thermal Degradation of Aqueous 2-Amino-2-methyl-1-propanol for CO2 Capture. *Energy Fuels* **2021**, *35*, 16705−16712.
(26) Yoon, B.; Hwang, G. S. Facile Carbamic Acid Intermediate Formation in Aqueous Monoethanolamine and Its Vital Role in CO2 Capture Processes. *Ind. Eng. Chem. Res.* **2022**, *61*, 4475−4479.
(27) Car, R.; Parrinello, M. Unified Approach for Molecular Dynamics and Density-Functional Theory. *Phys. Rev. Lett.* **1985**, *55*, 2471−2474.
(28) Perdew, J. P.; Burke, K.; Ernzerhof, M. Generalized Gradient Approximation Made Simple. *Phys. Rev. Lett.* **1996**, *77*, 3865−3868.
(29) Zhang, Y.; Yang, W. Comment on "Generalized Gradient Approximation Made Simple". *Phys. Rev. Lett.* **1998**, *80*, 890.
(30) Troullier, N.; Martins, J. L. Efficient Pseudopotentials for Plane-Wave Calculations. II. Operators for Fast Iterative Diagonalization. *Phys. Rev. B: Condens. Matter Mater. Phys.* **1991**, *43*, 8861−8869.
(31) Kleinman, D. M.; Bylander, L. Efficacious Form for Model Pseudopotentials. *Phys. Rev. Lett.* **1982**, *48*, 1425−1428.
(32) Smith, D. G. A.; Burns, L. A.; Patkowski, K.; Sherrill, C. D. Revised Damping Parameters for the D3 Dispersion Correction to Density Functional Theory. *J. Phys. Chem. Lett.* **2016**, *7*, 2197−2203.
(33) Gillan, M. J.; Alfè, D.; Michaelides, A. Perspective: How Good Is DFT for Water? *J. Chem. Phys.* **2016**, *144*, 130901.
(34) Yoshida, H. Construction of Higher Order Symplectic Integrators. *Phys. Lett. A* **1990**, *150*, 262−268.
(35) Evans, D. J.; Holian, B. L. The Nose-Hoover thermostat. *J. Chem. Phys.* **1985**, *83*, 4069−4074.
(36) Bonomi, M.; Branduardi, D.; Bussi, G.; Camilloni, C.; Provasi, D.; Raiteri, P.; Donadio, D.; Marinelli, F.; Pietrucci, F.; Broglia, R. A.; et al. PLUMED: A Portable Plugin for Free-Energy Calculations with Molecular Dynamics. *Comput. Phys. Commun.* **2009**, *180*, 1961−1972.
(37) Barducci, A.; Bussi, G.; Parrinello, M. Well-Tempered Metadynamics: A Smoothly Converging and Tunable Free-Energy Method. *Phys. Rev. Lett.* **2008**, *100*, 1−4.
(38) Dama, J. F.; Parrinello, M.; Voth, G. A. Well-Tempered Metadynamics Converges Asymptotically. *Phys. Rev. Lett.* **2014**, *112*, 1−6.
(39) Stowe, H. M.; Paek, E.; Hwang, G. S. First-principles assessment of CO2 capture mechanisms in aqueous piperazine solution. *Phys. Chem. Chem. Phys.* **2016**, *18*, 25296−25307.
(40) Yoon, B.; Hwang, G. S. On the mechanism of predominant urea formation from thermal degradation of CO2-loaded aqueous ethylenediamine. *Phys. Chem. Chem. Phys.* **2020**, *22*, 17336−17343.

https://doi.org/10.1021/acssuschemeng.2c02502
ACS Sustainable Chem. Eng. 2022, 10, 9584−9590